https://doi.org/10.15407/ujpe66.12.1048

R.M. BALABAI, V.M. ZDESCHITS, M.V. NAUMENKO

Kryvyi Rig State Pedagogical University
(54, Gagarina Ave., Kryvyi Rig 50086, Ukraine; e-mails: balabai@i.ua, valeriy.zdeschits@kdpu.edu.ua, nikemar13@gmail.com)

MECHANICAL MODIFICATION OF ELECTRONIC PROPERTIES OF ULTRATHIN β-Ga_2O_3 FILMS

Using the methods of the electronic density functional and pseudopotential theories, the spatial distributions of the valence electron density, the density of electronic states, and the gap widths in thin β-Ga_2O_3 films with various free surfaces subjected to mechanical compression are obtained from the first principles and using the author's program code. It is shown that the thickness of the β-Ga_2O_3 films, the type of their free surface, and the mechanical action of compression allow the conductive properties of β-Ga_2O_3 thin films to be controlled.

K e y w o r d s: β-Ga_2O_3 films, *ab initio* calculations, mechanical compression.

1. Introduction

Wide-band-gap materials – such as GaN, InGaN, and SiC – have been successfully developed during the last decade, thus affecting our everyday life. In particular, in the case of nitrides, they allowed the functionality of both electronic and optoelectronic devices to be enhanced. Nowadays, the relevant research is aimed at ultra-wideband semiconductor materials with the energy bandwidth exceeding 4 eV. There are a few such materials that attract special attention, namely, AlGaN, AlN, diamond, and β-Ga_2O_3. All of them belong to the class of so-called transparent oxides with semiconductor properties. Diamond is very difficult to produce in large amounts and with a high structural quality. Al-based nitrides also undergo technological difficulties when obtaining large quantities of high-quality crystals. Among those ultra-widegap semiconductor materials, only β-Ga_2O_3 can be grown in large amounts.

There are five Ga_2O_3 polymorphs [1]: of the corundum type (α), monoclinic (β), defect spinel (γ), orthorhombic (ε), and the δ-phase, which is considered to be orthorhombic. The β-phase (β-Ga_2O_3) has the most stable crystalline structure. It was and still remains the subject of most studies [2]. More important is the fact that β-Ga_2O_3 can be obtained directly from the melt using the scalable growth methods. The latter require lower production costs in comparison with the fabrication of other materials of this type.

The β-Ga_2O_3 material with its unique optical and electrical characteristics is considered to be an important complement to other ultra-wideband semiconductor materials in new application areas. The studies of β-Ga_2O_3 were initiated as long ago as in the 1960s, but later this material was almost forgotten for decades. Intensive research of β-Ga_2O_3 concerning its physical and functional applications, which was carried out within the last two decades, has brought this compound to the forefront of the development of ultra-wideband semiconductor materials. Various growth methods and epitaxial techniques were studied, followed by intensive research of the electrical, optical, thermal, and mechanical properties. The results of those studies have been documented in a large number of publications and patents [3–6].

Considerable attention is currently being paid to the epitaxial growth of β-Ga_2O_3 films [7]. Epitaxial gallium oxide is a new, although not yet fully studied, but very promising wide-band-gap semiconductor. It possesses a number of properties that make it a significant competitor to materials such as silicon carbide and nitrides of the third-group elements. First of all, this is its transparency in the ultraviolet spectral region because its band gap width amounts to $E_g \approx 4.9$ eV. In the crystalline state, this substance has a high breakdown voltage of 8 MV/cm. Gallium oxide can be easily doped, which makes it possible to obtain conductive layers of this material. β-Ga_2O_3 can be grown in large amounts and used in UV photodetectors, photocatalysts, gas sensors, solar panels, transparent conductive filters for electrodes of various optoelectronic devices, and so forth [8–19].

Two-dimensional (2D) Ga_2O_3 can extend the application scope of this compound. Nanodevices based on 2D Ga_2O_3 demonstrate a higher operational efficiency than nanodevices based on β-Ga_2O_3 do. However, the mechanisms of such a difference still remain not understood at length. According to previous studies, the characteristics of Ga_2O_3-based devices are substantially affected by the mechanical state of Ga_2O_3 [20]. An elastic field in a device arises in the course of thermal growing of Ga_2O_3, as well as due to a grating mismatch with other contacting materials, which is responsible for the thermal stability and transport properties of the material [21–31].

In the general case, the induction of deformation in two- and three-dimensional materials is a process of introducing the mechanical energy into the system. Within the elastic deformation limits, this energy is stored inside the material and leads to the appearance of nonequilibrium state, which results in a number of changes in the main properties of the material. If the elastic limit is exceeded, the energy can be released via the atomic rearrangement, the phase transition, or destruction. From the atomic viewpoint, pressure can change the initial state of atomic bond, by elongating or shortening the lengths of chemical bonds and modifying the lattice symmetry. As a result, the electronic structure of the material varies and, in turn, a number of physical properties also undergo considerable modifications [32]. Hence, deformation engineering is a simple and universal approach to the functionalization of material properties because it directly affects the atomic structure.

Thus, in order to further understand the characteristics and applications of 2D Ga_2O_3, it is necessary to analyze the mechanical effects on the electronic properties of this compound. In this work, modifications of the electronic properties of ultrathin β-Ga_2O_3 films with various free surfaces via mechanical actions were studied theoretically. Using the methods of the electronic density functional and pseudopotential theories, the spatial distributions of the valence electron density, the electronic state density, and the forbidden band gap width were obtained *ab initio* making use of the author's program code [32].

2. Calculation Models and Methods

The formalism of the electronic density functional (EDF) theory elaborated by Kohn, Hohenberg, and Sham is a powerful tool for calculating the electronic energy of molecules and solids. It is considered that the total energy of electrons moving in a given external potential can be obtained if the self-consistent electron density is known. While solving the Kohn–Hohenberg–Sham equations, the pseudopotential formalism can be applied, according to which a solid is considered as a combination of valence electrons and an ionic core. Among modern *ab initio* pseudopotentials obtained by inverting the Schrödinger equation for atoms, the Bachelet–Hamann–Schluter one [33] is widely used in solid-state calculations. This work is not an exclusion.

For non-periodic systems, such as defect crystals, thin films, or clusters, the problem of periodicity absence is avoided by means of the superlattice method [34], in which a supercell translated in space is created. When modeling non-periodic systems, such as thin films or clusters, the translated objects are isolated from one another making use of a vacuum gap between them.

The overall periodicity of the crystalline (or artificial) lattice creates a periodic potential and thus imposes the same periodicity on the electron density. The Kohn–Sham potential of a periodic system demonstrates the same periodicity as the lattice does, and the one-particle Kohn–Sham orbitals can be written in the Bloch form

$$\psi(\mathbf{r}) = \psi_i(\mathbf{r}, \mathbf{k}) = \exp(i\mathbf{kr})u_i(\mathbf{r}, \mathbf{k}), \tag{1}$$

where $\mathbf{k}$ is a wave vector from the first Brillouin zone (BZ) of the crystalline (or artificial) lattice. The sub-

script i enumerates all possible electronic states. The function $u_i(\mathbf{r},\mathbf{k})$ has the spatial periodicity of the lattice and can be expanded in a series of plane waves. This procedure substantiates the application of plane waves as a general basis chosen for the series expansion of the periodic part of orbitals. Since plane waves constitute a complete and orthonormal set of functions, the corresponding expansion of single-particle orbitals looks like

$$\psi_j(\mathbf{k},\mathbf{r}) = \frac{1}{\sqrt{N_0}\sqrt{\Omega}} \sum_{\mathbf{G}} b_j(\mathbf{k}+\mathbf{G}) \times \\ \times \exp\left(i\left(\mathbf{k}+\mathbf{G}\right)\mathbf{r}\right), \quad (2)$$

where $\mathbf{G}$'s are vectors in the reciprocal space, and $N_0\Omega$ is the volume of primitive cells filling the crystal or the artificial superlattice in the case of non-periodic objects.

After the Fourier transform, the one-particle Kohn–Sham equation has the following form in the reciprocal space:

$$\sum_{\mathbf{G}} \left[\left\{ \frac{\hbar^2}{2m} (\mathbf{k}+\mathbf{G})^2 - \varepsilon_j \right\} \delta_{\mathbf{G},\mathbf{G}'} + \right. \\ \left. + V_{\mathrm{KS}}(\mathbf{k}+\mathbf{G},\mathbf{k}+\mathbf{G}') \right] b_j(\mathbf{k}+\mathbf{G}) = 0, \quad (3)$$

where V_{KS} is the Kohn–Sham potential,

$$V_{\mathrm{KS}}(\mathbf{k}+\mathbf{G},\mathbf{k}+\mathbf{G}') = V_{PS}(\mathbf{k}+\mathbf{G},\mathbf{k}+\mathbf{G}') + \\ + V_H(\mathbf{G}'-\mathbf{G}) + V_{XC}(\mathbf{G}'-\mathbf{G}). \quad (4)$$

In the general case, the expressions describing the interaction potentials are complex-valued. The application of atomic bases containing the inversion operation in its point symmetry group makes the Fourier components real-valued in the expansion series of all expressions.

The main quantity in the EDF formalism is the electron charge density. It is estimated on the basis of a self-consistent solution of Eqs. (3). This solution must be obeyed at every point of the irreducible part of the BZ:

$$\rho(\mathbf{G}) = \frac{2}{N_T} \sum_k \sum_j \sum_{\alpha\in T} \sum_{\mathbf{G}} b_j^*(\mathbf{k}+\mathbf{G}'+\alpha\mathbf{G}) \times \\ \times b_j(\mathbf{k}+\mathbf{G}'), \quad (5)$$

where the subscript j enumerates all occupied states, $\mathbf{k}$ is a wave vector in the first BZ, N_T is the number of operations χ in the point group T of atomic basis, and the factor 2 takes into account the spin degeneracy.

The calculation efforts can be reduced by applying the method of special points. There are various approaches concerning the choice of those points. In particular, one may use uniform or non-uniform meshes of points. It is also possible with acceptable accuracy to replace summation over a finite number of special points or a single point in the BZ. The consideration can be confined only to the Γ-point in the BZ, which is especially effective in the case of artificial periodic systems with a large supercell.

The distribution of electrons over their energies is determined from the one-particle energy spectrum obtained after the diagonalization of the Kohn–Sham matrix (3) (the number of states in the spectrum depends on the size of the wave function expansion) by numerically calculating the derivative $\lim_{\Delta E\to 0}(\Delta N/\Delta E)$, where ΔN is the number of allowed states per energy interval ΔE. According to the EDF ideology, the number of occupied states at $T = 0$ K was determined as half the number of electrons in the atomic basis (due to the neglect of the electron spin).

Our calculation procedure was as follows. Instead of integration over the BZ, calculation at one BZ point, the Γ-point, was performed. Self-consistent iteration loops were terminated if the results of the current and previous iterations agreed with a given accuracy. Their number varied depending on the calculated object, but usually the iteration results agreed with each other after 3-5 loops. The limitation on the number of plane waves in the wave function expansion was made according to the results of trial calculations and by evaluating the physical sense of the obtained results (the spatial distribution of electron density, and the gap width between the top occupied state and the bottom unoccupied one in the electron energy spectrum) on the basis of general ideas obtained by other authors. Rather often, the number of plane waves was chosen to equal about 20–25 per basis atom.

Calculations of electronic properties are easier to carry out in the Cartesian space (X,Y,Z), whereas crystallographic symmetry operations are performed with the fractional crystallographic coordinates (x,y,z). In orthonormal crystallographic systems (cubic, tetragonal, and orthorhombic), the coordinate transformation is reduced to a simple nor-

malization of coordinate values by the corresponding cell constants, for example, $x = X/a$ and $X = ax$. In the case of the general oblique crystallographic system, the transformation requires matrix operations.

The monoclinic lattice of β-Ga_2O_3 [35] with the space group $C2/m$ includes two non-equivalently positioned Ga atoms [six-fold (Ga1) and four-fold (Ga2) coordinated ones] and three non-equivalently positioned O atoms [three-fold coordinated atoms O1 and O3, and four-coordinated atom O2]. The unit cell parameters of the lattice at room temperature are characterized by the values $a = 1.223$ nm, $b = 0.304$ nm, $c = 0.580$ nm, and the angle between the a- and c-axes $\beta = 103.7°$. Any unit cell contains four formula units, eight Ga atoms, and twelve O atoms, which fill the cell volume with two basis non-equivalently positioned Ga atoms and three basis non-equivalently positioned O atoms in the positions $4i$, $(0, 0, 0; 1/2, 1/2, 0)$ $(x, 0, z)$ [35–37] (see Table 1).

The fractional crystallographic coordinates of the atoms (they are quoted in Table 1) were transformed into the Cartesian coordinates using the algorithm described in our work [38]. The resulting positions of two basis non-equivalent Ga atoms (Ga1 and Ga2) and three basis non-equivalent O atoms (O1, O2, and O3) are shown in Fig. 1.

The symmetry operations of the Fedorov group $C2/m$ were used to construct the images of the basis (non-equivalent) atoms. As a result, the unit cell was filled with thirty atoms, which are shown in Fig. 2. Our transformation of the atomic coordinates from the crystallographic monoclinic system to the Cartesian one did not distort the crystal geometry. Therefore, the obtained set of atomic Cartesian coordinates can be used to calculate the characteristics of the electronic subsystem of the crystal using the author's computer program.

Table 1. **Non-equivalent fractional atomic positions in β-Ga_2O_3 [35]**

Atom	x	y	z	Coordination
Ga1	0.09050 (2)	0	0.79460 (5)	Four-fols
Ga2	0.15866 (2)	1/2	0.31402 (5)	Six-fold
O1	0.1645 (2)	0	0.1098 (3)	Three-fold
O2	0.1733 (2)	0	0.5632 (4)	Four-fols
O3	0.0041 (2)	1/2	0.2566 (3)	Three-fold

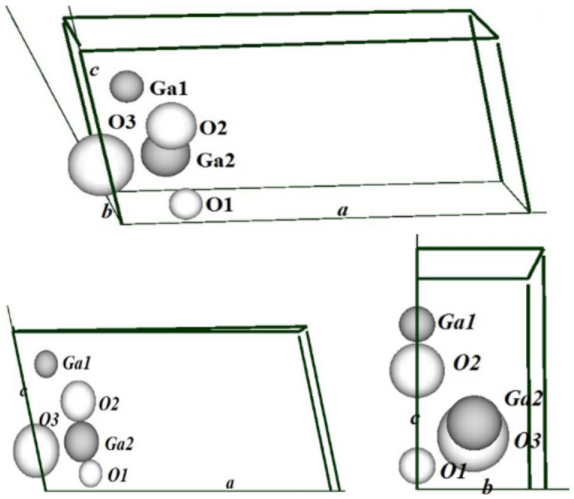

Fig. 1. Unit cell of β-Ga_2O_3 with two non-equivalently positioned basic Ga atoms (Ga1 and Ga2, gray spheres) and three non-equivalently positioned basic O atoms (O1, O2, and O3, white spheres) observed at various observation angles in the laboratory Cartesian coordinate system. The scheme was created with the help of the author's computer program

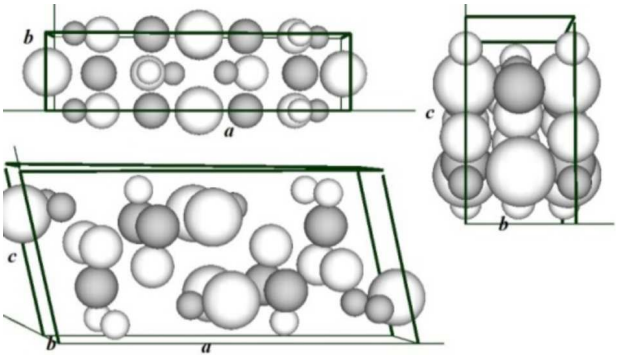

Fig. 2. Unit cell of β-Ga_2O_3 at various observation angles. The scheme was created in the laboratory Cartesian coordinate system using the author's computer program

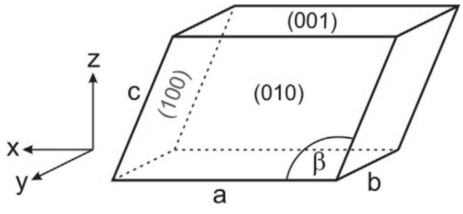

Fig. 3. Laboratory and crystallographic axes, and the planes that confine a unit cell

The conjugations of the laboratory and crystallographic axes and the planes confining the β-Ga_2O_3 unit cell are depicted in Fig. 3. The laboratory coor-

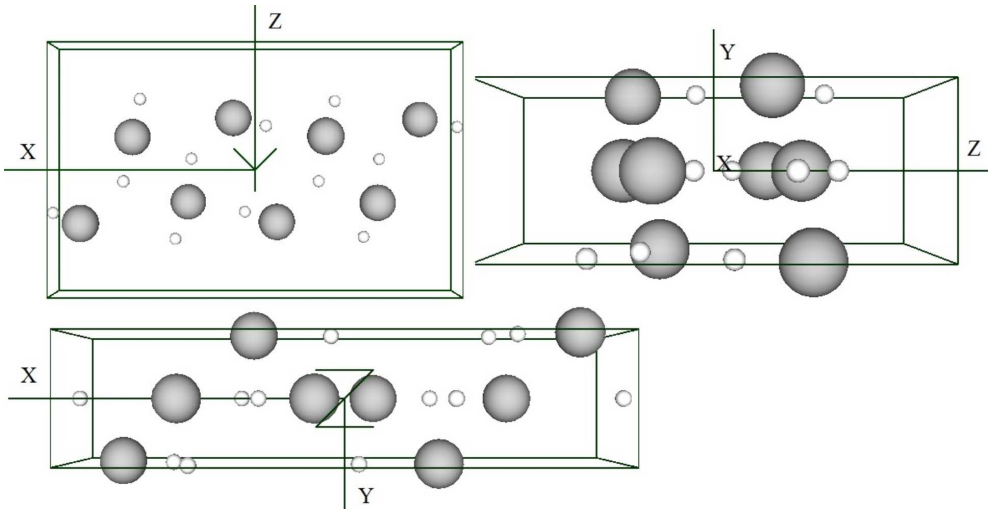

Fig. 4. Primitive cell of an artificial superlattice of the orthorhombic type, which reproduces the crystallographic space of an infinite β-Ga_2O_3 film with the monoclinic syngony, 0.439 nm in thickness, and with the (001) free surfaces

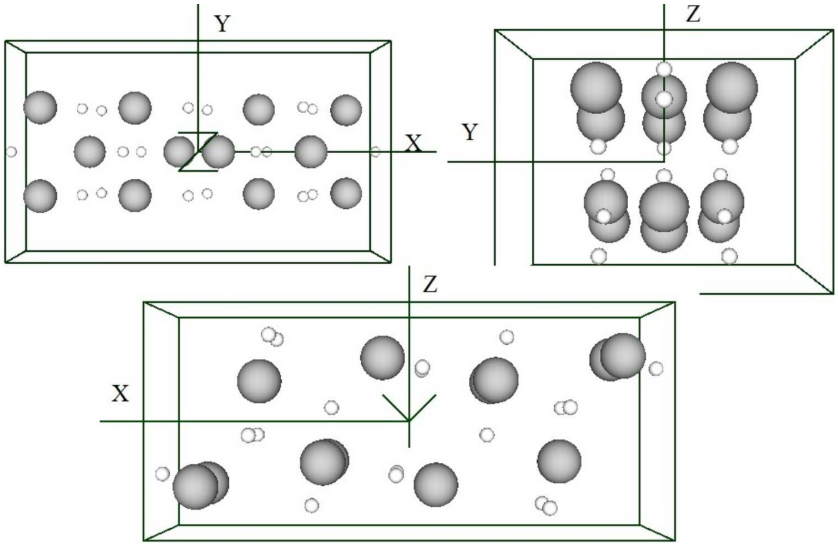

Fig. 5. Primitive cell of an artificial superlattice of the orthorhombic type, which reproduces the crystallographic space of an infinite β-Ga_2O_3 film with the monoclinic syngony, 0.304 nm in thickness, and with the (010) free surfaces

dinate system used in the author's software package was rectangular, and the calculation algorithm assumed the translational symmetry, Therefore, while studying the β-Ga_2O_3 atomic system, an artificial superlattice of the orthorhombic type was developed first, the primitive cell of which was a rectangular parallelepiped. A researched object determined the parameters of this superlattice and the atomic basis. We studied ultrathin β-Ga_2O_3 films with the free surfaces (010), (001), and (100). Therefore, the size of the primitive cell in the direction perpendicular to the free surfaces of β-Ga_2O_3 films was chosen so that the translationally repeating films would not affect one another through the built-in vacuum gaps. At the same time, in the plane parallel to the surfaces, the β-Ga_2O_3 films were infinite. In Fig. 4 to 6, the primitive

cells of the artificial superlattices of the orthorhombic type, which reproduce the crystallographic space of infinite β-Ga_2O_3 films of the monoclinic syngony with the spatial group $C2/m$ with various free surfaces are depicted. Ultrathin β-Ga_2O_3 films were assumed to retain the monoclinic character of their structure irrespective of their thickness.

The atomic basis of the primitive cell of the artificial superlattice (being translated, it reproduced the (001) β-Ga_2O_3 film) consisted of 20 atoms (8 Ga atoms and 12 O atoms), the atomic basis that reproduced the (010) β-Ga_2O_3 film consisted of 30 atoms (12 Ga atoms and 18 O atoms), and the atomic basis of the primitive cell reproducing the (100) β-Ga_2O_3 film at translation consisted of 20 atoms (8 Ga atoms and 12 O atoms). The surfaces of the (001) and (010) films were perfectly flat with a perfect crystalline arrangement, and they could be associated with epitaxially grown films. On the other hand, the surfaces of the (100) films were corrugated, and they could be associated with polycrystalline films, the grain size of which coincided with the unit cell size in β-Ga_2O_3.

The thicknesses of the model infinite films were 0.304, 0.439, and 1.29 nm for the films with the surface (010), (001), and (100), respectively. These are the thicknesses of the thinnest β-Ga_2O_3 films at which they preserve the peculiarities of the crystalline structure of this material. They can be interpreted as freely suspended films, which we really studied in this work to understand their characteristics and possible applications. For example, such films can be used as the main element in a pressure sensor, where an ultrathin and almost two-dimensional structure is freely suspended in the chamber in a position that allows the examined medium to affect both surfaces of the β-Ga_2O_3 film. The authors of work [39] reported on technological possibilities of manufacturing freely suspended β-Ga_2O_3-based nanoobjects of this kind.

3. Calculation Results and Their Discussion

The simulation of mechanical actions like static compression was performed by changing the corresponding atomic coordinates in the compression force direction. In particular, for the film with the (001) free surfaces, the compression force acted in the [001] direction conjugate to the Cartesian direction Z. Accordingly, the Z-coordinates of atoms decreased to 35% of the original values with a step of 5%. At the same time, for the film with the (010) free surfaces, the compression force acted in the [010] direction, which is conjugate to the Cartesian direction Y. Accordingly, the Y-coordinates of atoms decreased to 35% of the original values with a step of 5%. For the film with the (100) free surfaces, the compression force acted in the $[100]\cos(13.7°)$ direction, which is conjugate to the Cartesian direction X, and, accordingly, the X-coordinates of atoms decreased to 35% of the original values with a step of 5%.

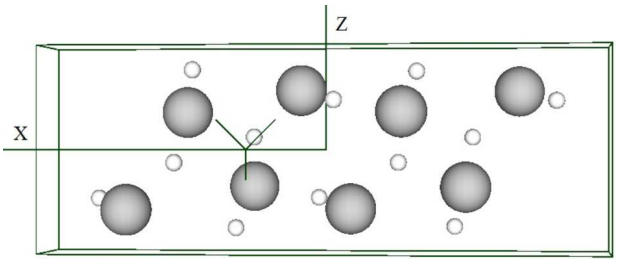

Fig. 6. Primitive cell of an artificial superlattice of orthorhombic type, which reproduces the crystallographic space of an infinite β-Ga_2O_3 film with the monoclinic syngony, 1.29 nm in thickness, and with the (100) free surfaces

The spatial distributions of valence electron densities, the electron state densities, and the band gap widths of model films were calculated *ab initio* using the EDF methods in the local and pseudopotential approximations. In so doing, the author's program code [32] was applied. The atomic basis was not optimized. The results calculated for the forbidden band gaps in the films at various mechanical compression levels are quoted in Table 2 and illustrated in Fig. 7.

The analysis of the obtained values makes it possible to state the following facts.

1. The film with the (010) surface is the thinnest one (0.304 nm) in comparison with the others (0.439 and 1.29 nm). It can be interpreted as a 2D object. In the initial (uncompressed) state, it has the largest band gap width among all studied films. The corresponding value is almost five times as large as the forbidden gap width in the massive β-Ga_2O_3 crystal.

2. The film with the (001) surface was also rather thin (0.439 nm). But in the initial (uncompressed) state, it has the narrowest band gap among all examined films, which is three times as narrow as the forbidden gap in the massive β-Ga_2O_3 crystal.

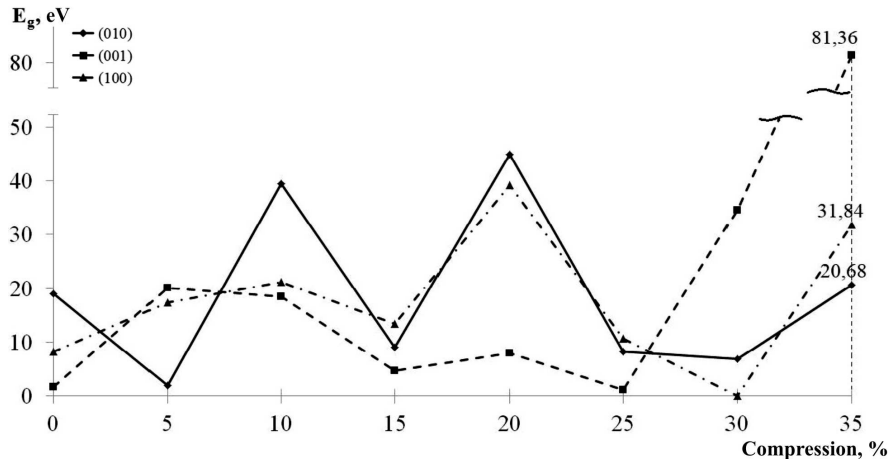

Fig. 7. Forbidden gap widths in infinite β-Ga_2O_3 films with various free surfaces – (010), solid curve; (001), dashed curve; and (100), dashed-dotted curve – at various mechanical compression levels

3. The film with the non-flat (100) surface was the thickest one (1.29 nm). Under mechanical compression, the changes in its band gap (its insignificant growth was observed) were the most monotonous among the other films (up to 15% at low compressions). At higher compressions, the monotonic behavior of the changes in the film band gap width disappeared and a drastic increase was registered at the compression to 20%. The further compression to 30% resulted in the band gap disappearance.

4. In the case of the thinnest film, which we interpreted as a 2D object, its compression led to substantial oscillations of the band gap width. A certain periodicity of those oscillations was observed, with a step of 10% of compression.

Table 2. **Band gap widths in infinite β-Ga_2O_3 films with various free surfaces and at various mechanical compression levels**

% compression	Film with the free surfaces		
	(010), eV	(001), eV	(100), eV
0	19.05	1.63	8.16
5	1.90	20.14	17.41
10	39.46	18.50	21.22
15	8.98	4.63	13.33
20	44.90	7.89	39.18
25	8.16	1.09	10.61
30	6.80	34.56	0
35	20.68	81.36	31.84

5. The band gap in the film with the (001) surface was the most responsive to the compression growth to 35% in comparison with other films. Its width grew by almost two orders of magnitude.

Thus, the thickness of the β-Ga_2O_3 film, the type of the film free surface, and the mechanical compression action on the film make it possible to affect and control the conductive properties of ultrathin β-Ga_2O_3 films. Our results of theoretical calculations are close to the conclusions drawn by the authors of work [7] that the mechanical properties of gallium oxide films vary considerably depending on the type of their growth surface.

As concerning the form of the spatial distributions of the valence electron densities in various films at various mechanical compression levels, they did not change qualitatively. Only a reasonable growth of the electron density was registered in the film bulk when the film thickness decreased at compression. It can be seen from the cross-sections of the spatial distributions of valence electrons (see, e.g., Fig. 8) as an increase in the intensity of the gray color in the image, followed by its transformation into black.

In Fig. 9, a selected oxygen atom from a primitive cell of an artificial superlattice reproducing the crystallographic space of an infinite β-Ga_2O_3 film of the monoclinic syngony with the (001) free surfaces is marked by an arrow. The evolution of the spatial distributions of the valence electron density in a vicinity of this atom under the mechanical compression of the film is exhibited in Fig. 10 in detail.

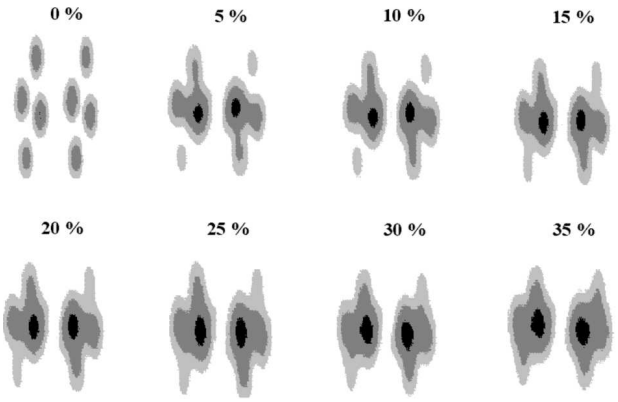

Fig. 8. Cross-sections of the spatial distributions of the valence electron density in a primitive cell of an artificial superlattice of the orthorhombic type, which reproduced the crystallographic space of an infinite β-Ga_2O_3 film with monoclinic syngony and the (001) free surfaces, at various mechanical compression levels of the film from 0 to 35%

Figures 8 and 10 demonstrate that under the compression action, the electron density becomes concentrated along the chemical bonds, thus counteracting the mechanical load; the chemical bonds become as if they are "strained"; the angles between the neighbor bonds and the length of the bonds themselves change (but without their catastrophic ruptures), which brings about the appearance of point defects or dislocations. This process was described in works [40, 41], where it was claimed that if the ideal structure of the crystal lattice becomes distorted, most of the bonds available in the defectless crystal survive, but they change and form configurations with turned bonds. This is called the orientational defect. Depending on the chemical composition of the material and, hence, the type of bonds between the atoms in the crystal, this specific feature manifests itself differently, but always affects the macroscopic physical characteristics of the object. The influence of the formed orientational defects in ultrathin β-Ga_2O_3 films with various types of free surfaces under the influence of mechanical compression distinctly reveals itself as a sharp and nonmonotonic change in the widths of electron band gaps (see Fig. 7). The availability of jumps in the values of the band gap widths is just associated with an extremely thin film thickness, when, in the course of a step-by-step model film compression, atomic shifts bring about a radically new organizational scheme of the orientational defects of chemical bonds. For massive films, this reaction is averaged over their thickness.

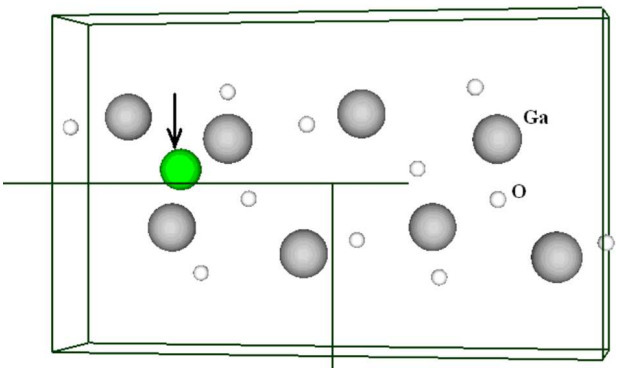

Fig. 9. Position of the selected oxygen atom (marked by an arrow) in a primitive cell of an artificial superlattice of the orthorhombic type, which reproduces the crystallographic space of an infinite β-Ga_2O_3 film with the monoclinic syngony and the (001) free surfaces

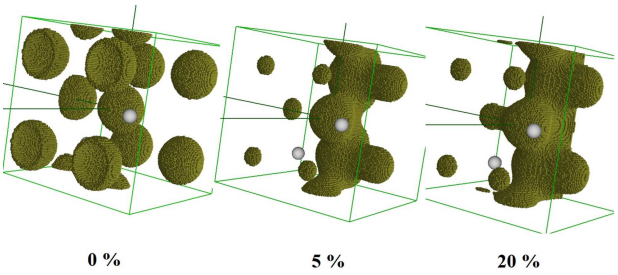

Fig. 10. Spatial distributions of the valence electron density for isovalues of 0.5–0.4 times the maximum value in the vicinity of the selected oxygen atom (Fig. 9) in an infinite β-Ga_2O_3 film with the (001) free surfaces various mechanical compression levels

Under real conditions, every specimen contains point defects and impurities, which play a crucial role for their conductivity. In future works, the indicated factors will also be taken into account and analyzed in the framework of the described model.

4. Conclusions

Using the *ab initio* electron density functional and pseudopotential methods, the spatial distributions of valence electron density, electron state density, and band gap width in ultrathin β-Ga_2O_3 films with the (010), (001), or (100) free surface subjected to mechanical compression have been calculated with the help of the author's program code. It is shown that the thickness of the β-Ga_2O_3 film, the type of the free

film surface, and the mechanical compression action allow the conductive properties of ultrafine β-Ga_2O_3 films to be affected and controlled.

It is found that the thinnest (0.304 nm) film with the (010) surface, which was interpreted as a 2D object, has the largest band gap in the initial (uncompressed) state among all other studied films, which is almost five times as large as the forbidden gap in the massive β-Ga_2O_3 crystal. The forbidden gap in the thickest (1.29 nm) film with the non-flat (100) surface is found to vanish, if the film was compressed to 30%.

The spatial distributions of the valence electron densities in the studied films had no qualitative changes in their organizations at various mechanical compression levels. The formation of orientational defects in ultrathin β-Ga_2O_3 films with various free surfaces under the action of mechanical compression manifests itself as a drastic and nonmonotonic change in their electron band gap widths.

1. R. Roy, V.G. Hill, E.F. Osburn. Polymorphism of Ga_2O_3 and the system Ga_2O_3–H_2O. *Am. Chem. Soc.* **74**, 719 (1952).
2. S.I. Stepanov, V.I. Nikolaev, V.E. Bougrov, A.E. Romanov. Gallium oxide: properties and application: A review. *Rev. Adv. Mater. Sci.* **44**, 63 (2016).
3. S.J. Pearton, Fan Ren, M. Tadjer, J. Kim. Perspective: Ga_2O_3 for ultra-high power rectifiers and MOSFETS. *Appl. Phys.* **124**, 220901-1-19 (2018).
4. M. Higashiwaki, K. Sasaki, A. Kuramata, T. Masui, S. Yamakoshi. Gallium oxide (Ga_2O_3) metal-semiconductor field-effect transistors on single-crystal β-Ga_2O_3 (010) substrates. *Appl. Phys. Lett.* **100**, 013504 (2012).
5. E.G. Villora, K. Shimamura, Y. Yoshikawa, K. Aoki, N. Ichinose. Large-size β-Ga_2O_3 single crystals and wafers. *J. Cryst. Growth* **270**, 420 (2004).
6. H. Aida, K. Nishiguchi, H. Takeda, N. Aota, K. Sunakawa, Y. Yaguchi. Growth of β-Ga_2O_3 single crystals by the edge-defined, film fed growth method. *Appl. Phys.* **47,** 8506 (2008).
7. Z. Feng, A.F.M. Anhar Uddin Bhuiyan, Md. Rezaul Karim, H. Zhao. MOCVD homoepitaxy of Si-doped (010) β-Ga_2O_3 thin films with superior transport properties. *Appl. Phys. Lett.* **114**, 250601 (2019).
8. S.A. Kukushkin, V.I. Nikolaev, A.V. Osipov, E.V. Osipova, A.I. Pechnikov, N.A. Feoktistov. Epitaxial gallium oxide on SiC/Si substrates. *Fiz. Tverd. Tela* **58**, 1812 (2016) (in Russian).
9. A.S. Grashchenko, S.A. Kukushkin, V.I. Nikolaev, A.V. Osipov, E.V. Osipova, I.P. Soshnikov. Study of the anisotropic elastoplastic properties of α-Ga_2O_3 films synthesized on SiC/Si substrates. *Fiz. Tverd. Tela* **60**, 851 (2018) (in Russian).
10. S.J. Pearton, Y. Jiancheng, P.H. Cary IV, F. Ren, J. Kim, M.J. Tadjer, M.A. Mastro. A review of Ga_2O_3 materials, processing, and devices. *Appl. Phys. Rev.* **5**, 011301 (2018).
11. N. Makeswaran, D. Das, V. Zade, P. Gaurav, V. Shutthanandan, S. Tan, C.V. Ramana. Size- and phase-controlled nanometer-thick β-Ga_2O_3 films with green photoluminescence for optoelectronic applications. *ACS Appl. Nano Mater.* **4**, 3331 (2021).
12. S. Ilhom, A. Mohammad, D. Shukla, J. Grasso, B.G. Willis, A.K. Okyay, N. Biyikli. Low-temperature as-grown crystalline β-Ga_2O_3 films via plasma-enhanced atomic layer deposition. *ACS Appl. Mater. Inter.* **13**, 8538 (2021).
13. X.C. Guo, N.H. Hao, D.Y. Guo, Z.P. Wu, Y.H. An, X.L. Chu, L.H. Li, P.G. Li, M. Lei, W. H. Tang. β-Ga_2O_3/p-Si heterojunction solar-blind ultraviolet photodetector with enhanced photoelectric responsivity. *J. Alloys Compd.* **660**, 136 (2016).
14. N. Suzuki, S. Ohira, M. Tanaka, T. Sugawara, K. Nakajima, T. Shishido. Fabrication and characterization of transparent conductive Sn-doped β-Ga_2O_3 single crystal. *Phys. Status Solidi C* **4**, 2310 (2007).
15. Z. Li, T. Jiao, J. Yu, D. Hu, Y. Lv, W. Li, X. Dong, B. Zhang, Y. Zhang, Z. Feng, G. Li, G. Du. Single crystalline β-Ga_2O_3 homoepitaxial films grown by MOCVD. *Vacuum* **178**, 109440 (2020).
16. T. Jiao, Z. Li, W. Chen, X. Dong, Z. Li, Z. Diao, Y. Zhang, B. Zhang. Stable electron concentration Si-doped β-Ga_2O_3 films homoepitaxial growth by MOCVD. *Coating* **11**, 589 (2021).
17. G. Joshi, Y.S. Chauhan, A. Verma. Temperature dependence of β-Ga_2O_3 heteroepitaxy on c-plane sapphire using low pressure chemical vapor deposition. *J. Alloys Compd.* **883**, 160799 (2021).
18. M.A. Mastro, A. Kuramat, J. Calkins, J. Kim, F. Ren, S.J. Pearton. Opportunities and future directions for Ga_2O_3. *ECS J. Solid State Sci. Tech.* **6**, 356 (2017).
19. X.H. Wang, F.B. Zhang, K. Saito, T. Tanaka, M. Nishio, Q.X. Guo. Electrical properties and emission mechanisms of Zn-doped β-Ga_2O_3 films. *J. Phys. Chem. Solids* **75**, 1201 (2014).
20. K. Adachi, H. Ogi, N. Takeuchi, N. Nakamura, H. Watanabe, T. Ito, Y. Ozaki. Unusual elasticity of monoclinic β-Ga_2O_3. *Appl. Phys.* **124**, 085102 (2018).
21. S. Krishnamoorthy, Z. Xia, S. Bajaj, M. Brenner, S. Rajan. Delta-doped β-gallium oxide field-effect transistor. *Appl. Phys. Expr.* **10**, 051102 (2017).
22. J. Su, R. Guo, Z. Lin, S. Zhang, J. Zhang, J. Chang, Y. Hao. Unusual electronic and optical properties of two-dimensional Ga_2O_3 predicted by density functional theory. *J. Phys. Chem. C* **122**, 24592 (2018).
23. J. Li, L. An, C. Lu, J. Liu. Conversion between hexagonal GaN and β-Ga_2O_3 nanowires and their electrical transport properties. *Nano Lett.* **6**, 148 (2006).
24. P. Jiang, X. Qian, X. Li, R. Yang. Three-dimensional anisotropic thermal conductivity tensor of single crystalline β-Ga_2O_3. *Appl. Phys. Lett.* **113**, 232105 (2018).

25. J. Su, J. Zhang, R. Guo, Z. Lin, M. Liu, J. Zhang, J. Chang, Y. Hao. Mechanical and thermodynamic properties of two-dimensional monoclinic Ga_2O_3. *Mater. Design* **184**, 108197 (2019).
26. K.-W. Ang, K.-J. Chui, V. Bliznetsov, C.-H. Tung, A. Du, N. Balasubramanian, G. Samudra, M.F. Li, Y.-C. Yeo. Lattice strain analysis of transistor structures with silicon-germanium and silicon-carbon source/drain stressors. *Appl. Phys. Lett.* **86**, 093102 (2005).
27. E. Chikoidze, D.J. Rogers, F.H. Teherani, C. Rubio, G. Sauthier, H.J. Von Bardeleben, T. Tchelidze, C. Ton-That, A. Fellous, P. Bove, E.V. Sandana, Y. Dumont, A. Perez-Tomas. Puzzling robust 2D metallic conductivity in undoped β-Ga_2O_3 thin films. *Mater. Today Phys.* **8**, 10 (2019).
28. S. Luan, L. Dong, R. Jia. Analysis of the structural, anisotropic elastic and electronic properties of β-Ga_2O_3 with various pressures. *J. Cryst. Growth* **505**, 74 (2019).
29. K. Adachi, H. Ogi, N. Takeuchi, N. Nakamura, H. Watanabe, T. Ito, Y. Ozaki. Unusual elasticity of monoclinic β-Ga_2O_3. *J. Appl. Phys.* **124**, 085102 (2018).
30. H. He, M.A. Blanco, R. Pandey. Electronic and thermodynamic properties of β-Ga_2O_3. *Appl. Phys. Lett.* **88**, 261904 (2006).
31. R. Ahrling, J. Boy, M. Handwerg, O. Chiatti, R. Mitdank, G. Wagner, Z. Galazka, S.F. Fischer. Transport properties and finite size effects in β-Ga_2O_3 thin films. *Sci. Rep.* **9**, 13149 (2019).
32. R. Balabai, A. Solomenko. Flexible 2D layered material junctions. *Appl. Nanosc.* **9**, 1011 (2019).
33. G.B. Bachelet, D.R. Hamann, M. Schluter. Pseudopotentials that work: from H to Pu. *Phys. Rev. B* **26**, 4199 (1982).
34. G. Makov, R. Shah, M.C. Payne. Periodic boundary conditions in ab initio calculations. II. Brillouin-zone sampling for aperiodic systems. *Phys. Rev. B* **53**, 15513 (1996).
35. J. Ahman, G. Svensson, J. Albertsson. A reinvestigation of β-gallium oxide. *Acta Cryst. C* **52**, 1336 (1996).
36. S. Geller. Crystal structure of β-Ga_2O_3. *J. Chem. Phys.* **33**, 676 (1960).
37. S. Kumar, R. Singh. Nanofunctional gallium oxide (Ga_2O_3) nanowires/nanostructures and their applications in nanodevices. *Phys. Status Solidi RRL* **7**, 781 (2013).
38. R.M. Balabai, M.V. Naumenko. Methodology of converting of the coordinates of the basis atoms in a unit cell of crystalline β-Ga_2O_3, specified in a monoclinic crystallographic system, in the laboratory cartesian coordinates for computer applications. *Photoelectronics* **29** (2020).
39. X.-Q. Zheng, J. Lee, S. Rafique, L. Han, C.A. Zorman, H. Zhao, Ph.X.-L. Feng. Free-standing β-Ga_2O_3 thin diaphragms. *Electronic Materials* **47**, 973 (2018).
40. R. Balabai, D. Kravtsova. Hardness of diamond-cBN nanocomposite. *Diamond Rel. Mater.* **82**, 56 (2018).
41. V.S. Vavilov, A.E. Kiv, O.R. Niyazov. *Mechanisms of Formation and Migration of Defects in Semiconductor*s (Nauka, 1981) (in Russian).

Received 22.01.21.
Translated from Ukrainian by O.I. Voitenko

Р.М. Балабай, В.М. Здещиц, М.В. Науменко

МОДИФІКАЦІЯ ЕЛЕКТРОННИХ ВЛАСТИВОСТЕЙ НАДТОНКИХ ПЛІВОК β-Ga_2O_3 МЕХАНІЧНИМИ ВПЛИВАМИ

Методами функціонала електронної густини та псевдопотенціалу, із перших принципів, з використанням авторського програмного коду отримано просторові розподіли густини валентних електронів, знайдено густини електронних станів, ширини заборонених зон у надтонких плівках β-Ga_2O_3 з різними вільними поверхнями під впливом механічного стиснення. Показано, що товщина плівки β-Ga_2O_3, тип вільної поверхні плівки та механічна дія стиснення дозволяють керувати провідними властивостями надтонких плівок β-Ga_2O_3.

Ключові слова: β-Ga_2O_3, плівки, розрахунки із перших принципів, механічне стиснення.